



Open Archive Toulouse Archive Ouverte (OATAO)

OATAO is an open access repository that collects the work of Toulouse researchers and makes it freely available over the web where possible

This is an author's version published in: <http://oatao.univ-toulouse.fr/25268>

Official URL: <https://doi.org/10.1016/j.ijpharm.2019.118692>

To cite this version:

Bushkalova, Raya  and Farno, Maylis  and Tenailleau, Christophe  and Duployer, Benjamin  and Cussac, Daniel and Parini, Angelo and Sallerin, Brigitte and Girod-Fullana, Sophie  *Alginate-chitosan PEC scaffolds: A useful tool for soft tissues cell therapy*. (2019) *International Journal of Pharmaceutics*, 571. 1-13. ISSN 0378-5173

Any correspondence concerning this service should be sent to the repository administrator: tech-oatao@listes-diff.inp-toulouse.fr

Alginate-chitosan PEC scaffolds: A useful tool for soft tissues cell therapy

Raya Bushkalova^{a,b}, Maylis Farno^{a,b}, Christophe Tenailleau^a, Benjamin Duployer^a, Daniel Cussac^{b,c}, Angelo Parini^{b,c}, Brigitte Sallerin^{b,c,d,1}, Sophie Girod Fullana^{a,*,1}

^a Université de Toulouse, CIRIMAT, UPS-INPT-CNRS, Faculté de Pharmacie, F-31062 Toulouse, France

^b INSERM, U1048, Toulouse F-31432, France

^c Université de Toulouse, UPS, Faculté des Sciences Pharmaceutiques, F-31062 Toulouse, France

^d CHU Toulouse, Pôle Pharmacie, Toulouse, F-31432, France

ARTICLE INFO

Keywords:

Alginate
Chitosan
Polyelectrolyte complex
Cell therapy
Mesenchymal stem cells
Biocompatibility
Angiogenesis

ABSTRACT

In this study we evaluate macroporous scaffolds made of alginate-chitosan polyelectrolyte complexes (PEC) as tools to optimize the results of soft tissues cell therapy. Cell therapy using mesenchymal stem cells (MSC) has become attractive for tissue repair and regeneration in a number of acute and chronic injuries. Unfortunately their low retention and/or survival after injection limit their beneficial effects. A biomaterial-assisted implantation, providing cells a three-dimensional (3D) microenvironment is a promising strategy. To this purpose, we designed a family of PEC scaffolds, and studied if they could meet the requirement of such application. X-ray tomography showed that all PEC scaffolds present an interconnected macroporosity, and both rheology and tensile measurements reveal optimized mechanical properties (higher storage moduli and Young moduli) compared to alginate reference scaffolds. In vitro assays demonstrated their ability to allow MSC retention (higher than 90%), long-term viability and FGF2 secretion. Then, we used a skeletal muscle implantation model to assess the biological response to scaffolds graft, and showed that they support in vivo vascular formation within the implant-derived tissue. The combination of alginate/chitosan PEC scaffolds architecture and angiogenic potential make them appear as interesting tools to optimize MSC therapy results in soft tissues.

1. Introduction

In recent years, cell therapy using Bone Marrow Mesenchymal Stem Cells (BM MSC) has become an attractive tool for tissue repair and regeneration in a number of acute and chronic injuries. Although the first studies in the field suggested that the beneficial effects of administered BM MSC might be related to their terminal differentiation in the host cell type, this mechanism of action is controversial. In contrast, it is now well established that BM MSC promote repair of injured tissues through the secretion of a variety of paracrine growth (basic fibroblast growth factor [b FGF], insulin like growth factor 1 [IGF1], hepatocyte growth factor [HGF]) immunomodulatory (interleukine 10 [IL 10]) and angiogenic (vascular endothelial growth factor α [VEGF α]) factors (Shologu et al., 2018). They act as mini pumps secreting locally factors whose properties are particularly attractive for the remission of ischemic injury. In particular, we (Mias et al., 2009) and others (Gnecchi et al., 2006) supported the importance of FGF produced by BM MSC in promoting tissue repair after renal (Mias et al., 2009) and cardiac

(Gnecchi et al., 2006) ischemia. Furthermore, we have already shown that MSCs encapsulated in alginate scaffolds maintain their capacity to produce FGF2 (Trouche et al., 2010) and VEGF, FGF2, HGF, EGF, IGF 1 and G CSF after 28 days of encapsulation (Ceccaldi et al., 2012; Ceccaldi et al., 2017), and retain their initial phenotype and ability to differentiate later under a differentiating medium (Trouche et al., 2010; Ceccaldi et al., 2012).

The benefits of BM MSC therapy has been demonstrated in the management of ischemic damage of several tissues including heart (Hare et al., 2009; Williams and Hare, 2011; Karantalis et al., 2014 and Bartunek et al., 2013; Mias et al., 2009; Amsalem et al., 2007; Feygin et al., 2007; Perin et al., 2008), kidney (Mias et al., 2008; Qi and Wu, 2013; Reis et al., 2012; Tögel and Westenfelder, 2012), lung (Souidi et al., 2013), liver (Pan et al., 2012; Chen et al., 2012; Wang et al., 2014), vasculature (Poitevin et al., 2014) and brain (Li et al., 2005; Chopp et al., 2009). In these studies, BM MSC have been delivered by systemic intravenous infusion or injected into the targeted organ. However, data from preclinical and clinical trials suggest that their

* Corresponding author at: Laboratoire de Pharmacie Galénique, CIRIMAT, UMR 5085 UPS-INPT-CNRS, Institut Carnot, Equipe "Phosphates, Pharmacotechnie, Biomatériaux", Faculté des Sciences Pharmaceutiques, 31062 Toulouse cedex 09, France.

E-mail address: sophie.fullana-girod@univ-tlse3.fr (S. Girod Fullana).

¹ These authors provided equal contribution to this work (last author).

intravascular or intraparenchymal injection results into a low rate of retention and/or survival. Intravenous perfusion is hampered by low retention rates within 24 h of delivery, typically < 10%, and a long term survival and engraftment < 1% (Mäkelä et al., 2015; Malliaras and Marbán, 2011; Cheng et al., 2013). Direct intraparenchymal injections results in better retention of cells, but leads to poor survival rates, generally < 1% (Toma et al., 2002; Feygin et al., 2007; Morigi et al., 2008; Cheng et al., 2013; Wang et al., 2014).

To address the need for increased retention and better viability of transplanted cells, a promising strategy is to associate MSCs with a biocompatible material that protects and concentrates them on the damaged area (Noronha et al., 2019). For tissue engineering applications, macroporous scaffolds are of particular interest since they allow improved cell invasion and rapid exchange of nutrients, oxygen and metabolic wastes, while providing the scaffold seeded cells a three dimensional (3D) microenvironment. As a consequence scaffold's design is decisive to optimize cell therapy results. Key requirements include control of scaffold's porosity, mechanical properties, and biocompatibility. It has been established that pore size and distribution affect the biological performance of the construct by influencing cell morphogenesis (Zmora et al., 2002), cell behaviors and host cell colonization (Zeltinger et al., 2001; Salem et al., 2002). Therefore, the ideal scaffold should present an interconnected porosity with pore sizes compatible with 3D cell culture. In addition, the ideal scaffold should present mechanical properties that not only suit the specific application (according to the mechanical characteristics of the targeted organ) but also allow surgical manipulation during grafting.

Natural polymers seem to be particularly adapted for the elaboration of cell carrier systems due to both their structural properties and high biocompatibility. Alginates are among the most commonly used biopolymers in regenerative medicine due to their structural similarities with the extracellular matrix, their gelling properties under conditions compatible with biological activities (37 °C, pH 7.4 ...) and their low cytotoxicity. They are naturally occurring anionic linear (unbranched) polysaccharides, which can be extracted from kelp, brown seaweed and some bacteria. In terms of chemical structure, alginates are salts of alginic acid consisting of 1,4 linked β -D-mannuronic (M) and α -L-guluronic (G) residues organized in regions of sequential G units (G blocks), sequential M units (M blocks) and G and M units atactically organized. Their sol gel transition properties are based on the formation of a stiff "egg box" structure due to divalent cations selective binding to the G blocks of two adjacent polymeric chains. A number of studies have demonstrated the benefits of alginate 3D scaffolds seeded with various cell types for the regeneration of heart (Zieber et al., 2014; Dvir et al., 2009; Leor et al., 2000), liver (Dvir Ginzberg et al., 2008) and kidney (Kim et al., 2003). Although this therapeutic approach seems promising, the use of alginate macroporous scaffolds as implantable devices is challenged by drawbacks such as fragility (Ceccaldi et al., 2012) and lack of specific signals for cell attachment (Shachar et al., 2011). Strategies to improve alginate properties may entail chemical modifications leading to potentially toxic reactive intermediates. One alternative to chemical modification is to associate alginate with a cationic polymer like chitosan, to form polyelectrolyte complexes of opposite charge (PEC) with improved properties. Chitosan is a cationic copolymer of 2-acetamido-2-deoxy-D-glucopyranose and 2-amino-2-deoxy-D-glucopyranose, obtained by deacetylation of naturally occurring chitin. Chitosan is a biocompatible and biodegradable polymer whose applications in the tissue engineering field include regeneration of bone and articular cartilage (Malafaya and Reis, 2009; Ahmed and Hincke, 2014), heart (Hussain et al., 2013; Wang et al., 2010), kidney (Gao et al., 2012), skin (Azad et al., 2004), and nervous tissue (Gnavi et al., 2013; Zahir et al., 2008).

Use of alginate/chitosan porous scaffolds has been described mainly in the field of bone and cartilage tissue engineering (Florczyk et al., 2013; Li et al., 2015; Li and Zhang, 2005; Qi et al., 2011; Li et al., 2008; Shao and Hunter, 2007; Li et al., 2005) due to the increased mechanical

properties of the obtained PEC (in the range of several MPa). The use of PEC formation has more rarely been reported for soft tissue applications. In a previous study, we have shown that a combination of process and formulation parameters can lead to a family of alginate chitosan PEC scaffolds suitable for cardiac applications (Ceccaldi et al., 2014). In this study, we explore if these scaffolds could match the specifications for soft tissue treatment by MSC. We hypothesized that biomaterial design can lead to a construct whose architecture could permit good cell retention and viability combined with angiogenic potential. To this purpose, we designed alginate/chitosan PEC scaffolds with controlled porosity and mechanical properties and demonstrated their ability to allow MSC retention, long term viability and FGF2 secretion in vitro. Next, as a proof of principle, we used a skeletal muscle implantation model to assess the biologic effect of the obtained constructs to support in vivo vascular formation within the implant derived tissue.

2. Materials and Methods

2.1. Materials

Sodium alginate (molecular weight 80,000-120,000; ratio M/G = 1.56), chitosan (molecular weight 190,000-310,000; 84.6% deacetylated), HEPES sodium salt, Dulbecco's Phosphate Buffered Saline (DPBS) without calcium chloride and magnesium chloride, as well as antibiotics penicillin streptomycin were purchased from Sigma Aldrich, France. Calcium chloride dihydrate ($\text{CaCl}_2 \cdot 2\text{H}_2\text{O}$) and sodium chloride (NaCl) were purchased from VWR. Fetal Medium for cell culture was prepared by supplementing the MEM α with 10% fetal bovine serum and 1% penicillin streptomycin.

2.2. Preparation of Alginate/Chitosan Macroporous 3D Scaffolds

Three dimensional alginate/chitosan PEC scaffolds (containing alginate/chitosan weight ratio of 60/40, 50/50 and 40/60) were prepared by a freeze drying technique following a method reported previously (Ceccaldi et al., 2014). Briefly, 100 μ l of polyelectrolyte solutions or 200 μ l of single polymer solution (pure alginate (ratio 100/0) or of pure chitosan (ratio 0/100) 1.5% w/w, used as controls) were placed in a 96 well plate, frozen overnight at -20 °C and lyophilized. Constructs were cross linked in an isotonic buffer (pH 7.4) containing 150 mM NaCl, 0.1 M $\text{CaCl}_2 \cdot 2\text{H}_2\text{O}$, and 12.5 mM HEPES during 1 h. Pure chitosan scaffolds were cross linked with NaOH 1 M. All scaffolds were washed 2 times during 1 h in a HEPES buffer (pH 7.4), and lyophilized again. The final scaffolds dimensions, used in all experiments, were 5 mm diameter \times 2.5 mm thickness.

2.3. Physico chemical Characterization

2.3.1. Computed X ray Micro tomography (Micro CT)

The micro CT study of samples was carried out on Phoenix Nanotom 180 (GE Sensing, Germany) using the following parameters: 30 kV voltage, 160 microA current, no filter material, 0.25° rotation step, 5 frames as frame averaging, 1440 tomographic projections over a 360° scan angle, 1 s exposure time. A binning 2 \times 2 was applied for the slices reconstruction and the resulting voxel size was 11.5 μm^3 . Three dimensional virtual models of scaffolds were obtained using VGStudio MAX 2.1. A region of interest (ROI) was drawn within the reconstructed volume and a threshold was defined to identify the polymeric phase. Then, a morphometric analysis of the ROI was performed to obtain the total porosity and void interconnectivity. Scaffolds' morphologies were analyzed on the basis of 2D X ray tomographic slices using ImageJ (NIH, USA). Calculations were done on a ROI defined on the surface and in the cross section of each scaffold. Feret's diameters were obtained and pore densities were calculated as the total void number/ROI area ($n = 10$ slices per scaffold). Voids on edges were excluded.

2.3.2. Swelling

The swelling behaviors of the scaffolds were studied at room temperature by measuring their weights in a dry (W_{dry}) and in a wet (W_{wet}) state using an electronic balance. A dry scaffold was placed in a mesh basket and then immersed in an excess of culture medium. At regular time intervals the basket containing the wet scaffold was taken out of the medium, drained on an absorbent paper and weighed. The swelling ratio was calculated using the following formula:

$$\text{Swelling ratio} = (W_{wet} - W_{dry})/W_{dry}$$

2.3.3. Rheological Characterization

Rheological measurements were carried out using a stress controlled rheometer (Rheostress RS75, HAAKE, Germany) with a parallel plate geometry. Test samples matching the diameter of the plate (20 mm) were prepared. After complete rehydration in culture medium, the specimens were carefully laid on absorbent paper to remove excess liquid before lowering the rheometer top plate. Stress sweeps at a constant frequency of 1 Hz were first performed to obtain the linear viscoelastic region for collecting subsequent data. Then, frequency sweeps were performed in the linear viscoelastic regime to determine the storage modulus (G') and the loss modulus (G'').

2.3.4. Tensile Testing

The scaffolds' tensile properties were evaluated through a uniaxial tensile test performed using a TA XT2 Texture Analyzer (Stable Microsystems, UK) with tensile grips. Specimens were cut as a self designed dumbbell shape (100 mm total length, 60 mm gage length, 8.7 mm gage section), then completely rehydrated in culture medium at room temperature. Excess liquid was removed on tissue paper and the shoulders were fixed between the tensile grips. The specimens were stretched at a constant speed of 2 mm/s and stress strain curves were recorded until rupture. Tensile strength at 30% of elongation were calculated.

2.4. In Vitro Assays

2.4.1. Isolation and Culture of Rat Bone Marrow MSCs

Mesenchymal stromal cells were obtained from the femurs of Lewis male rats (Harlan, France) weighing 180–200 g as previously described (Ceccaldi et al., 2014; Mias et al., 2009). Briefly, anesthesia was performed by intraperitoneal injection of pentobarbital (0.1 ml/100 g) before animals were euthanized. Bone marrow was flushed from rat's femur with MEM α supplemented with 10% fetal bovine serum and 1% penicillin/streptomycin, and centrifuged (300 \times g, 5 min). Then cells were plated in culture flasks (10,000 cells/cm²). After 3 days, non adherent cells were removed by changing the culture medium, and MSCs were recovered by their capacity to adhere to plastic culture dishes. MSCs are qualified with the expression of surface markers such as CD90/Thy1, CD29/Integrin alpha 9 beta 1, CD106/VCAM 1 and their capacity to differentiate into adipocytes, chondrocytes, and osteocytes in culture. MSCs were then routinely cultured and were used for the experiments between the third and the sixth passage.

2.4.2. MSCs Seeding on Scaffolds

Each scaffold was placed in the well of a 96 well polystyrene plate and seeded by adding drop wise 10 μ l of cell suspension containing 100,000 MSCs (for in vitro experiments) or 500,000 MSCs (in vivo study) on the top of the scaffold. The plate was centrifuged 1 min at 400 \times g, and then 290 μ l of culture medium was added. The constructs were cultured in a 5% CO₂ incubator at 37 °C. For in vitro culture, the medium was changed every 2–3 days.

2.4.3. Live/Dead Assay and Confocal Microscopy

Live/Dead assays were performed using the Viability/Cytotoxicity Assay kit (FluoProbes[®], Interchim, France). After 1, 3, 7 and 15 days of

in vitro culture constructs were washed two times with a mix of MEM α and physiological serum (ratio 1/1). Staining solution containing 2 μ M ethidium homodimer 3 (necrotic marker measuring nucleus membrane integrity) and 1 μ M calcein AM (viability marker measuring the intracellular esterase activity) was prepared in a mix of MEM α and physiological serum 1/1 to stain dead cells in red and live cells in green. Scaffolds were incubated in the staining solution during 30 min in the dark at room temperature, then washed twice with DPBS and immediately observed under a confocal microscope Zeiss LSM510 using a 10 \times objective. The samples were excited with a 488 nm Argon laser and with a 543 nm helium neon laser. The emitted fluorescence was collected using two separate photomultiplier tubes with a BP 500–560 nm filter for calcein detection and a LP 620 nm filter for ethidium homodimer 3 detection. The 3D reconstructions were generated using Image J (NIH, USA) from microscopic images where the green and red channel were merged.

2.4.4. Evaluation of Cell Retention After Seeding Within 3D Scaffolds

The efficiency of cell retention after seeding within scaffolds was evaluated by measuring the total lactate dehydrogenase (LDH) activity of cell seeded scaffolds (3D) and of cells left at the bottom of the well (residual) using the Pierce LDH Cytotoxicity Assay Kit (Thermo Scientific). Sixteen hours after seeding, the scaffolds were immersed into a lysis solution and then the total LDH activity was measured according to the manufacturer's instructions. Absorbance was read at 450 nm (specific signal) and 620 nm (background signal) using a plate reading spectrophotometer (Infinite[®] 200Pro, Tecan Group). After subtraction of the background signal, cell retention efficiency was calculated as follows:

$$\text{Retention efficiency (\%)} = 1 - (\text{LDH}_{\text{residual}} / (\text{LDH}_{\text{residual}} + \text{LDH}_{3D})) \times 100.$$

In addition, a standard curve was established using scaffolds seeded with a known number of MSCs (culture medium and acellular scaffolds served as blank). All measurements were performed in triplicates.

2.4.5. Cell Proliferation in Scaffolds

MSC proliferation in different 3D scaffolds was assessed by measuring the double stranded genomic DNA content. On 0, 1, 3, 7 and 14 days of culture, the scaffolds were taken out of the culture plate wells, placed in Eppendorf tubes containing one 5 mm stainless steel bead each, and grinded using a mixer mill (Retsch). After that, total DNA was extracted using the GenElute Mammalian Genomic DNA Miniprep Kit (Sigma Aldrich) as specified by the manufacturer.

Finally, double stranded DNA content was quantified using the PicoGreen assay (Life Technologies). One hundred microliters of the eluate, containing pure genomic DNA, were transferred to a flat black 96 well plate and the fluorescence was measured at an excitation wavelength of 485 nm and an emission wavelength of 535 nm using a plate reader (Infinite[®] 200Pro, Tecan Group).

In parallel, two standard curves were established: one curve using purified double strand DNA (DNA diluting buffer was used as blank) and another curve using DNA extracted from scaffolds seeded with a known number of MSCs (acellular scaffolds were used as blank). All measurements were performed in triplicates.

2.4.6. Scanning Electron Microscopy (SEM)

40/60 PEC scaffolds were seeded with MSCs and cultured in vitro in cell culture medium according to the protocol previously described. After 3 days of culture, the samples were fixed in 3% glutaraldehyde in 0.1 M cacodylate buffer at 4 °C. The samples were subsequently coated under vacuum with platinum alloy, then immediately flash carbon coated under vacuum. The surfaces of the cell seeded scaffolds were examined in an ESEM Quanta 250 FEG FEI scanning electron microscope at an accelerating voltage of 5 kV and a magnification of 7000 times.

2.4.7. RNA Extraction and Real time Quantitative Reverse Transcription PCR (RT qPCR)

Total RNA was isolated from MCSs cultured in 2D or in 3D. Cell pellets or scaffolds were placed in Eppendorf tubes containing buffer RLT and 10% of β mercaptoethanol and then grinded using a mixer mill (Retsch) in the presence of 5 mm stainless steel bead. After that, total RNA extraction was performed using the RNeasy Mini Kit® (Quiagen) as specified by the manufacturer. RNA concentration was determined by measuring the absorbance at 260 nm in a NanoDrop® ND 1000 spectrophotometer.

RNA (300 ng per assay tube) was reverse transcribed to cDNA using the RT SuperScript II reverse transcriptase (Invitrogen). RT qPCR was performed on StepOne+ (Applied Biosystems) using SYBR® Premix EX Taq™ (Thi RNaseH Plus), Rox Plus (TaKaRa Bio) for detection of rat FGF2 and rat GAPDH (glyceraldehyde 3 phosphate dehydrogenase). The reaction assay mix contained 3 ng of cDNA (1:10 diluted template cDNA), 0.2 μ M of primers (Eurogentec) and the SYBR® Premix Ex Taq II, ROX Plus for a final volume of 10 μ l per well. Quantification of the housekeeping rat cDNA GAPDH was used as an internal control.

The absence of contaminants was checked by RT qPCR assays of negative control samples in which the Superscript II was omitted. Melting curve analysis was performed to ensure purity of the PCR products. Relative quantification was determined using the comparative CT method with data normalized to GAPDH. Experiments were performed in duplicate and results were treated with the StepOne Software v2.4 (Applied Biosystems). The sense and antisense primers used are:

Gene GAPDH (rat): Forward primer sequence: 5' AGGTCGGTGTGAACGGATTG 3'; Reverse primer sequence: 5' TGTAGACCATGTAGTTGAGGTCA 3'.

Gene FGF2 (rat): Forward primer sequence: 5' GTGTGTGCGAACC GGTACCT 3'; Reverse primer sequence: 5' TATTGGACTCCAGCGCTTCAA 3'.

2.4.8. Western Blot Analysis of Protein Expression

Protein extracts from MSCs cultured in 2D were obtained by cell lysis in a lysis buffer composed of DPBS 1 \times , 1% NP40 (IGEPAL®), 12 mM sodium deoxycholate, 0.1% SDS, and supplemented with a protease inhibitor. After centrifugation (10 min, 12,000 \times g, 4 °C) the supernatant and the pellet are separated. The pellet is suspended in a Tris SDS lysis buffer (pH 6.8) composed of 0.08 M Trizma® base (Sigma Aldrich), 5% SDS and 10% glycerol. Protein extracts from MSCs cultured in 3D scaffolds were obtained after a homogenization in a mixer.

2.5. In Vivo Assays

2.5.1. 3D scaffolds implantation

Animal experimentations were conducted in accordance with the European Communities Council Directive (2010/63/UE) for experimental animal care and were approved by local animal care and use committees C2EA 122 (Comités D'éthique En Expérimentation Animale). Rats were housed in an air conditioned room (SPF status) with 12 h light and dark cycles in a controlled environment at a temperature of 22 \pm 2 °C and a relative humidity of 45%. The animals occupied ventilated cages (3 animals / cage) with free access to food and water ad libitum. The bedding material is made of poplar litter and the environment is enriched. Furthermore, the animals were observed daily to assess the clinical state and behavior for the welfare related assessments. Concerning the experimentations, a randomization has been done to elicit each group.

Animals were under general anesthesia (3% isoflurane) and mechanical ventilation. 3D PEC scaffolds were implanted in adult female Lewis rats (200–220 g). After the skin was prepped and sterilized with ethanol, a small incision (about 1.3 cm) was made on the chest. The Pectoralis major muscle was exposed and a small muscle pouch was

formed between two sets of muscle fibers using surgical scissors. Animals were randomly divided into 2 groups. The 'Patch' group ($n = 8$) received a 40/60 PEC scaffold. Sham operated animals ($n = 5$) were subjected to the same surgical procedure without scaffold implantation. Finally, the muscle pouch was closed by a stitch. The implanted scaffolds had been hydrated for at least 12 h in MEM α under sterile conditions and their final dimensions were 5 mm diameter \times 2.5 mm thickness. The surgical procedure was realized under a Zeiss OPM1 FC microscope.

2.5.2. C reactive Protein Quantification

Measurements of C reactive protein (CRP) concentrations as an acute phase reactant were performed on blood collected by retro or bital bleeding on anesthetized rats from the two different experimental groups described above using heparinized tubes. Blood samples were centrifuged 15 min at 400 \times g and then the plasma was collected. CRP concentrations in plasma were evaluated using the xMAP technology (Luminex 100™ system, Luminexcorp) with the ProcartaPlex Rat CRP kit (eBioscience).

2.5.3. Histology

Histological analyses were performed on muscle specimens fixed in paraformaldehyde (4% solution in DPBS, pH 7.4) and embedded in paraffin.

For basic histomorphological evaluation, paraffin sections (4 μ m thick) were stained with hematoxylin and eosin according to standard protocols and slides were scanned using NanoZoomer Digital Pathology.

For immunofluorescence analyses, paraffin sections were dewaxed, rehydrated and incubated in a Tris EDTA antigen retrieval solution (10 mM Trizma® base, 1 mM EDTA, 0.05% Tween20, pH 9) at 121 °C for 3 min. After a permeabilization step (0.5% Triton 100 \times), nonspecific antigen sites were saturated for 30 min with a DPBS solution containing 2% of goat serum and 1% of bovine serum albumin. Sections were stained overnight with a mouse monoclonal anti α SMA (clone 1A4, Sigma Aldrich, 1:1000, 4 °C) and a polyclonal rabbit anti VWF (A0082, Dako, 1:200, 4 °C). Antibody detection was performed using Alexa Fluor® 568 goat anti mouse and AlexaFluor® 488 goat anti rabbit (Life Technologies, 1:200, 30 min). Cell nuclei were stained by DAPI (Sigma Aldrich, 0.05 μ g/ml, 10 min). Finally, sections were mounted with Fluoromount mounting medium (Sigma Aldrich).

Immunostained slides were photographed using a confocal Zeiss LSM 780 microscope. Blood vessel density (number of vessels per mm²) was determined by combining counting of α SMA positive structures and morphological analysis. At least five randomly selected images of the implanted area stained by a SMA fluorescent antibody were quantified for each animal.

2.6. Statistical Analyses

Statistical analyses were performed using GraphPad Prism 4 (Prism GraphPad, San Diego, CA). Results are expressed as mean \pm SEM. Statistical comparisons between two unpaired groups were performed using the *t* test (for data following a Gaussian distribution) or the Mann Whitney test (for data not following a Gaussian distribution). For the plasmatic CRP quantification, before after comparisons were performed using the Wilcoxon matched pairs test. Comparisons between more than two groups were performed using a one way ANOVA with Tukey's post test or using a Kruskal Wallis test with the Dunnett's post test (in case of a non Gaussian distribution). The influence of two factors was determined using two way ANOVA with Bonferroni's post test. A value of $p < .05$ was considered significant.

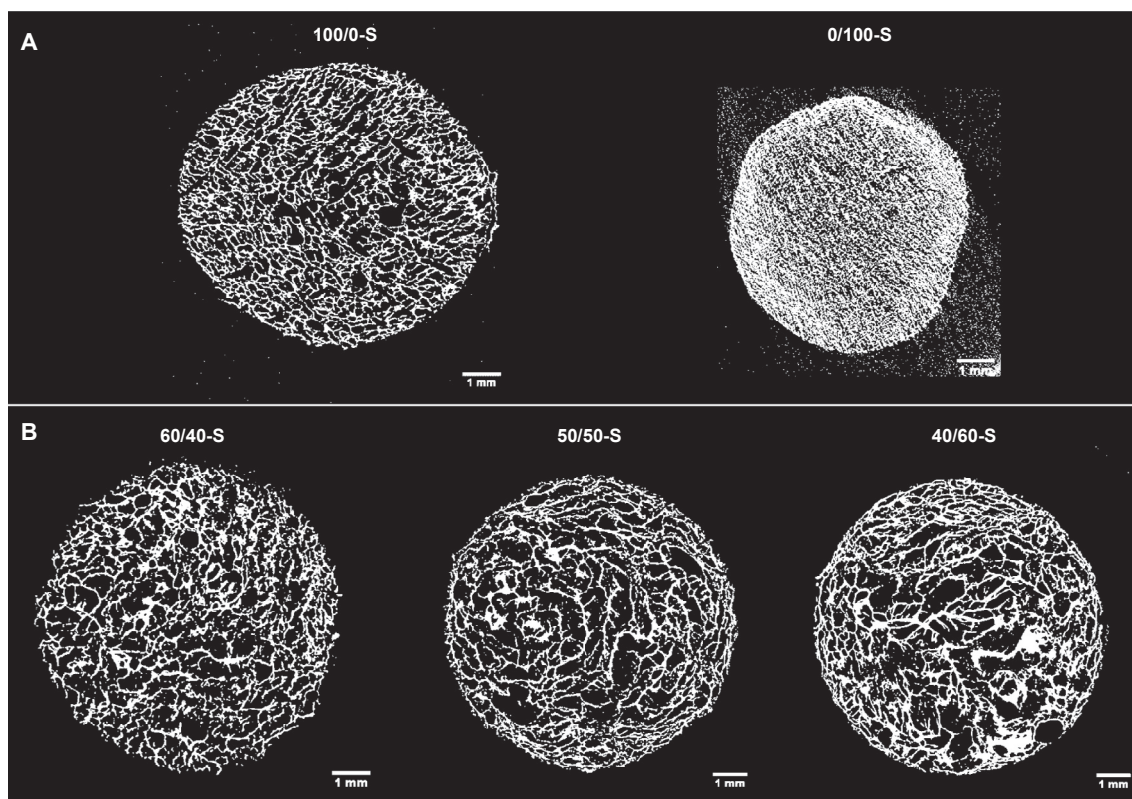


Fig. 1. Micro-CT analysis of the scaffolds: 2D micro-CT images of their cross-section. A: reference alginate (100/0-S) and chitosan (0/100-S) scaffolds; B: PEC scaffolds with various alginate/chitosan ratios 60/40 (60/40-S), 50/50 (50/50-S), and 40/60 (40/60-S). The scale bar is 1 mm for both panels (A and B).

3. Results

3.1. Alginate/Chitosan 3D PEC Scaffolds Physico chemical Characterization

3.1.1. 3D PEC Scaffolds Porous Architecture

Three different PEC scaffold types with a constant alginate concentration (1.5% w/w) and containing 60/40, 50/50 and 40/60 alginate/chitosan ratios (w/w) were prepared. In parallel, control scaffolds composed of pure alginate (1.5% w/w, defined as 100/0 alginate/chitosan ratio) or with pure chitosan (1.5% w/w, defined as 0/100 alginate/chitosan ratio) were prepared according to the same procedure.

Fig. 1 shows micro CT 2D slices reconstructions of alginate/chitosan PEC scaffolds in comparison with alginate and chitosan ones, and Table 1 summarizes porosity quantification data. All scaffolds were found to present a homogeneous morphology characterized by a highly interconnected macroporous structure. Morphometric analysis showed that all PEC scaffolds presented 100% interconnected pores and a total porosity equal or above 80%, significantly higher than 0/100 S (chitosan scaffolds; total porosity of 63%). The reconstructed scaffolds' slices reveal bigger pores and denser walls for PEC scaffolds in comparison with reference ones. This can be attributed to alginate/chitosan PEC

presence, distributed within the scaffolds.

Concerning pore sizes, measurements on micro CT slices showed average pore sizes between 170 and 201 μm for PEC scaffolds. They exhibited larger pore sizes than reference scaffolds, with a significant difference with chitosan reference 0/100 S. Pore density, spanning from 17 to 10 pores per squared millimeter, significantly decreased with raising the chitosan ratio within the PEC formulations (Table 1).

3.1.2. 3D PEC Scaffolds Swelling Behavior

With the goal to determine the time needed by the scaffolds to rehydrate after MSC deposit, their swelling kinetics have been studied. The obtained dried scaffolds readily absorbed culture medium and swelled quickly. Their swelling kinetics, presented in Fig. 2, show that within the first 5 min of rehydration the scaffolds have reached their maximal swelling ratio, which remained stable afterwards. All scaffolds preserved their morphology after rehydration and no scaffold degradation was observed within the 2 h of the experiment. However, PEC scaffolds' swelling ratios were significantly lower and present less variability than those measured for alginate and chitosan reference scaffolds, probably due to the stable ionic interactions between chitosan and alginate chains.

Table 1

Porosity quantification data on micro-CT reconstructions: mean pore diameter, mean pore density, porosity and voids interconnectivity of PEC and reference scaffolds.

Alginate/chitosan 3D scaffold	100/0-S	60/40-S	50/50-S	40/60-S	0/100-S
Mean pore diameter (μm)	149 \pm 4	170 \pm 4	201 \pm 5	194 \pm 6	77 \pm 1
Mean pore density (mm^{-2})	20.4 \pm 0.4	16.5 \pm 0.6	13.7 \pm 0.1	10.2 \pm 0.4	19.3 \pm 0.4
Porosity (%)	83	80	82	82	63
Voids interconnectivity (%)	100	100	100	100	100

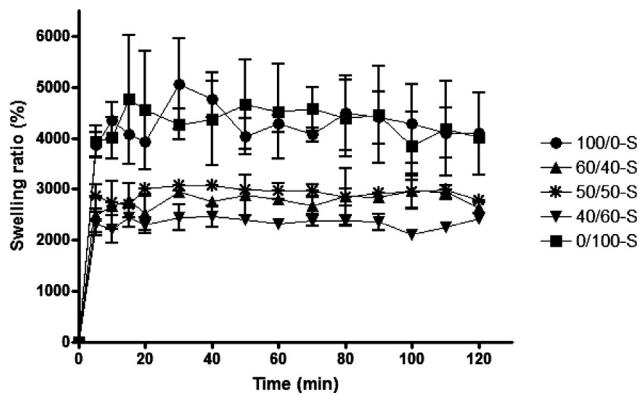


Fig. 2. Stability upon rehydration of the scaffolds: swelling ratios of reference and PEC 3D scaffolds as a function of sample immersion time in cell culture medium.

3.1.3. 3D PEC Scaffolds Viscoelastic Properties

Swollen scaffolds' rheological properties were studied in dynamic conditions in their linear viscoelastic zone at a shear rate of 10 Pa (Fig. 3). For all scaffolds the storage modulus (G') was higher than the loss modulus (G'') over a large frequency zone (between 10 and 0.01 Hz), which indicates the existence of viscoelastic gels with predominant elastic behavior. In addition, the existence of a plateau for G' and G'' in this frequency range reveals the formation of well structured hydrogels. G' values of PEC scaffolds increased proportionally to chitosan ratio; they are typically 10 to 12 times higher than G' of reference alginate scaffold. For 50/50 S and 40/60 S, the values of storage modulus at 0.5 Hz were even higher than values for reference chitosan scaffold 0/100 S (50/50: 17058 Pa, 40/60: 24767 Pa, 0/100: 13833 Pa).

3.1.4. 3D PEC Scaffolds Mechanical (Tensile) Properties

Mechanical behaviors of the PEC and reference scaffold were evaluated in swollen state using a uniaxial tensile test (Fig. 4). We observed that for all scaffolds elongation is more or less linear until break and that the linear region is longer when chitosan content is higher. In addition, the higher the chitosan percentage, the neater the break. PEC scaffolds presented increased Young's moduli compared to control alginate scaffold, as expected, due to the synergistic interactions between

the opposite charged polymers.

3.2. MSC Seeded Alginate/Chitosan 3D PEC Scaffolds: In Vitro Assays

3.2.1. MSC Viability, Retention and Proliferation Within Alginate/Chitosan 3D PEC Scaffolds

3D scaffolds were seeded with 100,000 MSCs and examined for cell viability, retention, and proliferation.

Cell viability was evaluated by confocal imaging 1, 3, 7 and 15 days post seeding using the Live/Dead[®] staining. Volume reconstructions of sequential z plane images, starting from the scaffold surface, are presented in Fig. 5. We observed that MSC viability was preserved during the 15 days of in vitro culture, as judged by the cells' bright green fluorescent staining and the virtually absent red staining. Furthermore, no significant difference was found in cell viability within the different types of scaffolds during the whole in vitro culture period. On the contrary, substantially higher cell densities were observed within PEC scaffolds compared with control alginate scaffolds. Indeed, within PEC scaffolds cell density was quite similar to that observed within chitosan scaffold 0/100 S, which is known to favor cell adhesion. Moreover, within PEC scaffolds cells presented a particular 3D distribution where they formed clusters seeming strongly related to the formation and 3D distribution of polyelectrolyte complexes (previously observed in micro CT).

Seeding efficiency was measured by quantifying the total LDH activity of cell seeded scaffolds and of cells left at the bottom of the well within 16 h of cell deposition. Our results show that the seeding efficiency was very high, above 90%, for all scaffold types (Fig. 6A). Within PEC scaffolds the seeding procedure reproducibility was greater compared to control alginate and chitosan scaffolds.

Cell proliferation was measured over 2 weeks by quantifying the amount of genomic DNA per scaffold (Fig. 6B). After one day of 3D culture, MSC number within 40/60 S was maintained identical to the number of cells used for seeding (95%), but not within control scaffolds (minus 50% in 100/0 S and minus 30% in 0/100 S). At the end of the two week period, cell number within 40/60 S was maintained similar to the number of initially seeded cells. In contrast, within 100/0 S and 0/100 S cell number globally decreases all over the experience. At every time point, cell number within 40/60 S was significantly superior to that in 100/0 S and remained close and even higher to that within 0/100 S. The cell loss between day 3 and day 7 within 40/60 S was followed by an increase in cell number by day 14 when it reached its

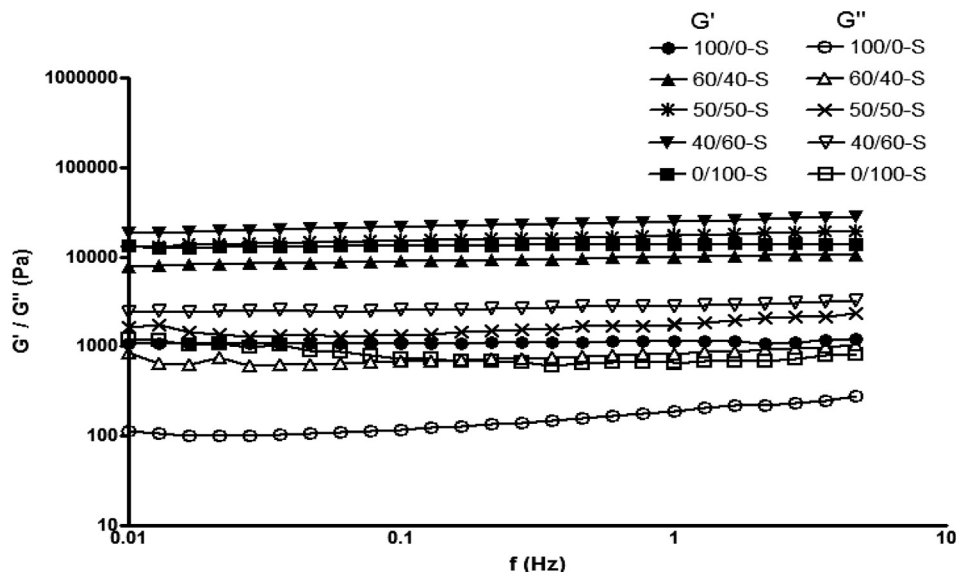


Fig. 3. Viscoelastic properties of reference and PEC 3D scaffolds in their fully swollen state: storage (G') and loss (G'') moduli according to frequency sweeps in the linear viscoelastic regime.

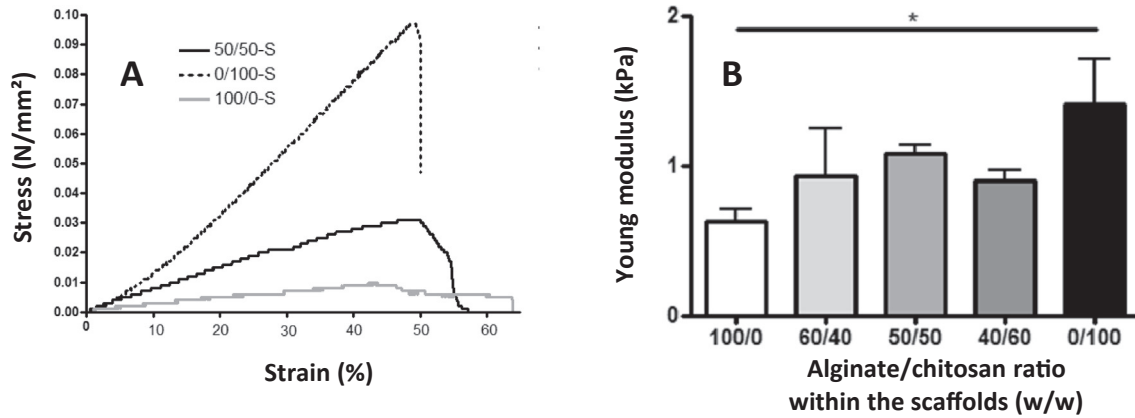


Fig. 4. Mechanical behavior of the scaffolds in their fully swollen state using a uniaxial tensile test. A: stress versus strain curves of alginate reference scaffold (100/0-S), chitosan reference scaffold (0/100-S) and a 50/50 PEC scaffold (50/50-S); B: Young's moduli in traction of the 3D scaffolds according to alginate/chitosan ratio. *: $p \leq .05$, based on two-way Anova analysis.

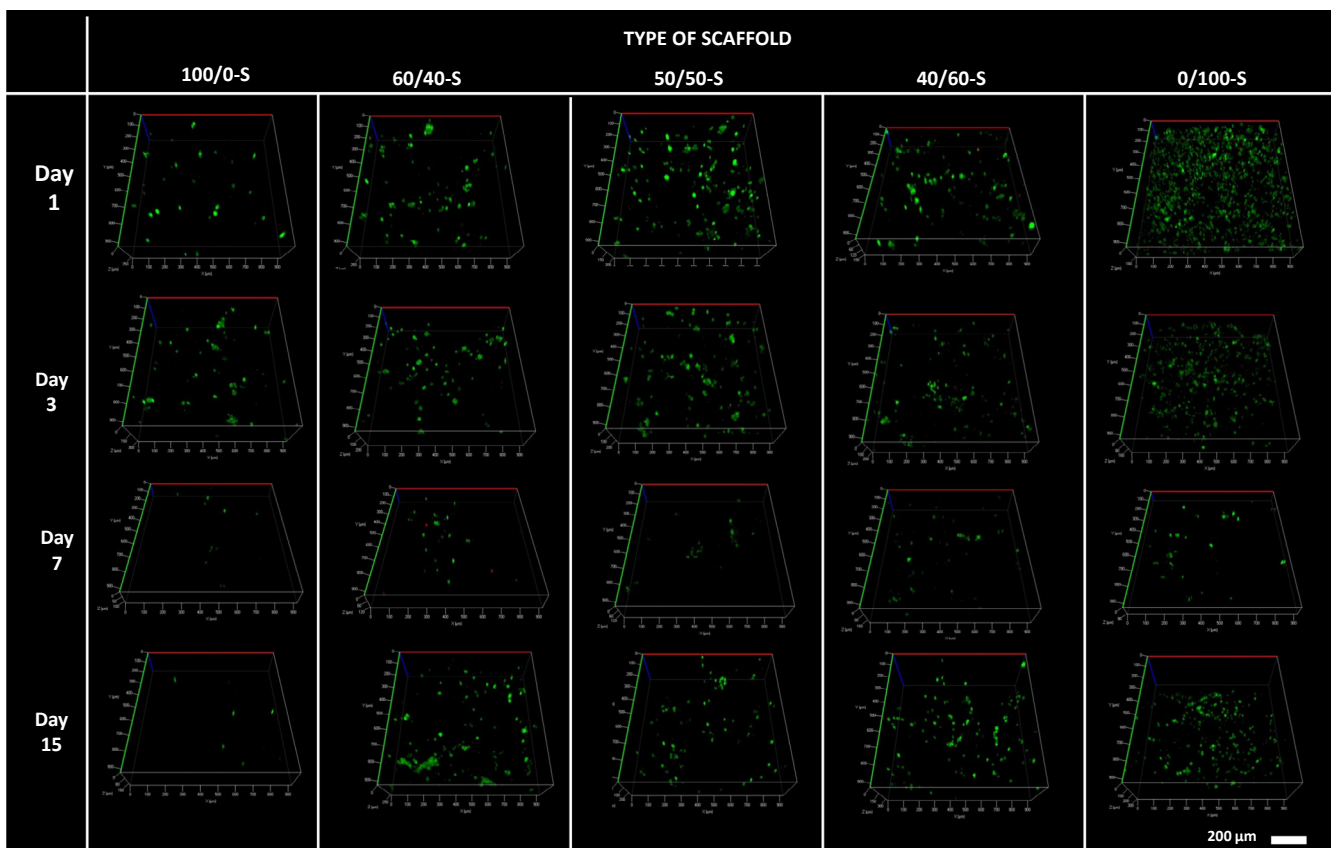


Fig. 5. Cell seeding of rat MSC cultured within reference and PEC 3D scaffolds. Confocal z-planes (from the surface: 1 to the bottom: 10) of MSC-seeded scaffolds observed after a Live/Dead staining (live cells in green and dead cells in red) 1, 3, 7 and 15 days after seeding. The scale bar is 200 μm . Each photo refers to green and red channels at each time point. (For interpretation of the references to colour in this figure legend, the reader is referred to the web version of this article.)

initial value at the moment of seeding. These results suggest that MSC proliferate within 40/60 S, contrary to 100/0 S and 0/100 S.

SEM imaging at high magnification revealed the cellular morphology on the 40/60 S surface three days after seeding (Fig. 7). At this time point the matrix is densely populated with fairly round shaped cells, with a diameter of about 3 μm , presenting numerous fibrillar extensions connecting them to the support (cell matrix interactions) and to neighbouring cells (cell cell interactions). (Fig. 7A). A closer view (Fig. 7B; zoomed area) shows that these cells adhered to the matrix by mean of microvillus extensions of the cytoplasm forming larger "feet" for adhesion to the scaffold. Cells were tightly caught with

a fiber network that we believe results from cell surface proteins' in interactions with the 3D scaffold components. Cell cell interactions were also noted via microvillus extensions between neighbouring MSCs.

Taken together, the in vitro experimental results indicate that PEC formation endows new properties of 3D scaffolds which are beneficial for MSC culture on the long term compared with alginate and chitosan alone. Indeed, 40/60 S favors not only cell viability, but also cell adhesion and proliferation. Therefore, we selected this formulation for further tests.

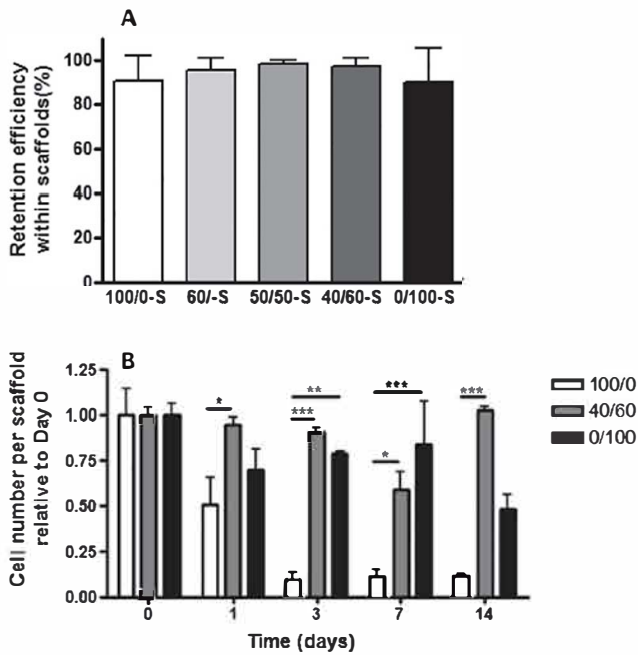


Fig. 6. A: MSC retention efficiency of the 3D scaffolds; B: MSC viability within 3D scaffolds. * denotes a significant difference compared to rat MSC on a culture plate (*: $p \leq .05$, **: $p \leq .01$, ***: $p \leq .001$, based on Anova analysis).

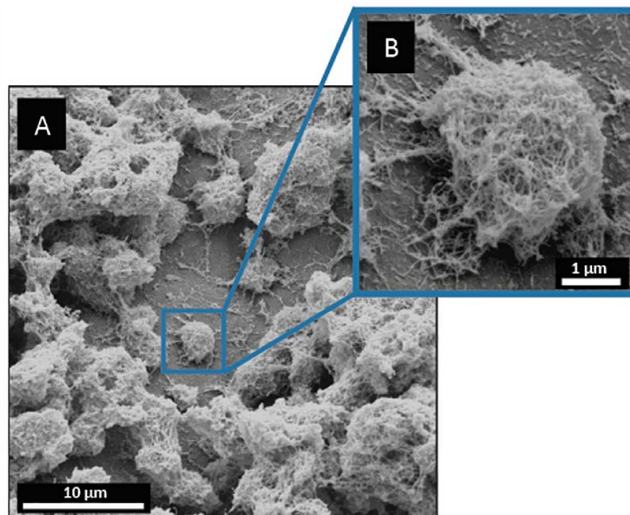


Fig. 7. Scanning electron microscopy examination of MSC seeded within 40/60 PEC scaffold (40/60-S) after 3 days of in vitro culture. A: overview; B: zoom on an MSC. The scale bar is 10 µm for panel A and 1 µm for panel B.

3.2.2. FGF2 MSC Secretion Ability Within 40/60 PEC Scaffolds

We investigated the FGF2 secretion in 3D culture conditions by quantification in the culture medium of MSC seeded within 40/60 PEC 3D scaffolds. Analyses were performed 24 h after seeding and results were compared to the amount measured in 2D.

We performed Western blot analyses on whole cell lysates (Fig. 8A and B) and also checked the expression levels for FGF2 mRNAs by reverse transcription and quantitative PCR (Fig. 8C). We found that FGF2 protein and FGF2 mRNA expressions were slightly higher within 40/60 PEC scaffold (40/60 S) than in 2D culture conditions, thus clearly showing that 40/60 PEC scaffolds permit to maintain and even have a tendency to promote FGF2 MSC secretion ability.

3.3. 40/60 PEC Scaffold In Vivo Biocompatibility and Vascularization After Implantation

As a proof of concept, we implanted the 40/60 PEC scaffold in a muscle pouch on the pectoral muscle of healthy rats to investigate its biocompatibility and angiogenic properties. Host tissue's reaction and graft's fate were monitored at 9 and 28 days after implantation.

All surgical incisions healed without evidence of infection. No significant differences in white blood cells level were observed between the control group and the acellular scaffold group (data not shown). Inflammation secondary to scaffold grafting was evaluated through the quantification of plasmatic C reactive protein (CRP) and no significant differences were observed in concentrations between the experimental groups along the study (Table 2). As an example, CRP values were $465 \pm 12 \mu\text{g/ml}$ for the control group and $467 \pm 68 \mu\text{g/ml}$ for the acellular scaffold group at day 9. These results show that the animals did not present systemic infection nor inflammation.

In order to evaluate host's immune reaction, as well as scaffold's engraftment and vascularization, grafts were harvested post mortem and stained with hematoxylin eosin or immunostained for alpha SMA and VWF.

Hematoxylin eosin stained sections on Fig. 9 reveal tissue response to scaffold implantation. The 40/60 PEC 3D scaffold appear well integrated within the muscular tissue 28 days post implantation (Fig. 8A). Grafts' biodegradation gradually progressed over time and the new tissue integrated well with adjacent muscles. At this time point a large number of small functional blood vessels (diameter 15–20 µm) containing erythrocytes were present between the degrading biomaterial fragments. The fibrous capsule was reduced to a thin (about 15 µm thick) and vascularized interface between the biomaterial and the muscular tissue (arrows on Fig. 9B and C). These results demonstrate the resolution of the inflammatory process and excellent tissue engraftment of 40/60 S.

In vivo vascularization of the implanted constructs was analyzed by staining for VWF and alpha SMA to detect endothelial cells and smooth muscle cells. Examination of immunostained sections revealed the presence of blood vessels throughout the granular tissue resulting from the implant's biodegradation. The number of SMA positive vessels/mm² was 166 ± 11.4 . This result indicates that alginate chitosan PEC 40/60 scaffolds support vascularization, a very important fact.

4. Discussion

One of the major challenges in the field of soft tissues cell therapy is to design strategies allowing the administration of stem/progenitor cells taking the maximum advantage of their therapeutic properties by increasing their survival and paracrine activities and decreasing their potential side effects. To that aim, the interest of a scaffold to improve the administration and optimize cell survival is now widely recognized. In this field, polymers of natural origin are widely used because of a variety of advantages, such as their good biocompatibility and biodegradability, and the similarity of their networks with the extracellular matrix. According to the previous reports, collagen, gelatin, alginate, chitosan, hyaluronic acid, agarose, and fibrin are the common biopolymers applied (Asgharia et al., 2017; Newsom et al., 2019; Tiwari et al., 2019; Li et al., 2019; Kaiser and Coulombe, 2015; Perez Estenaga et al., 2018; Rane and Christman, 2011; Perez et al., 2017; Lev and Seliktar, 2018; Liu et al., 2019; Saberianpour et al., 2018).

The main limitation of the scaffolds obtained from biopolymers is their lack of sufficient mechanical properties for handling and implantation, and their porosity, which is initially too low to allow cellular invasion. Different techniques can be used to strengthen biopolymers' networks, including chemical modifications and crosslinking (Oryana et al., 2018). However, these solutions, if they lead to mechanically stronger structures, are often at the expense of biocompatibility due to the use of solvents, and potentially toxic reaction

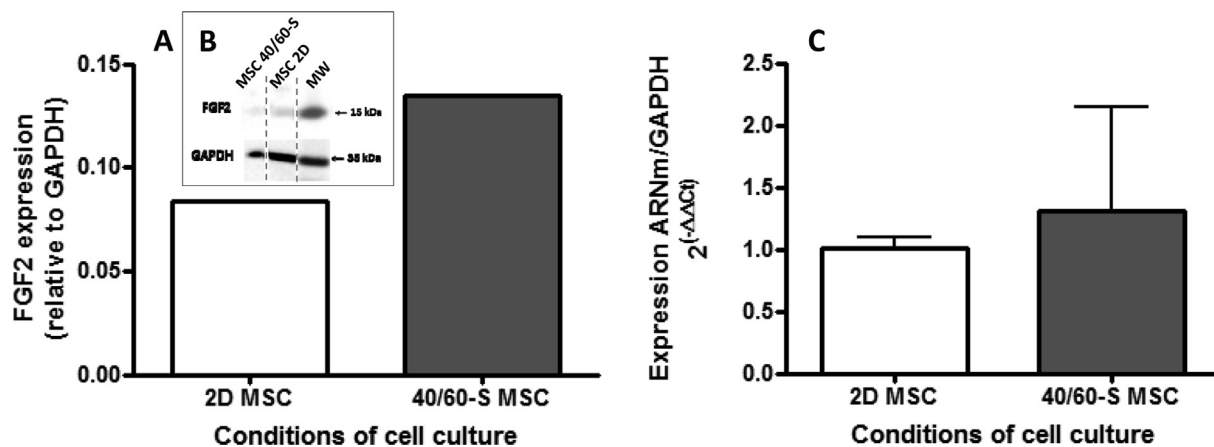


Fig. 8. FGF2 secretion ability of MSC cultured within 40/60 PEC scaffold or in culture plate 24 h post-seeding. A: quantification by Western blot of FGF-2 expression; B: corresponding image from the Western blot; C: expression levels for FGF2 mRNAs by reverse transcription and quantitative PCR.

Table 2

Plasmatic C-reactive protein (CRP) quantification at D0, D9 and D28 post implantation for control (sham) group and acellular PEC scaffold (40/60-S) group.

CRP (µg/ml)	D0	D9	D28
Sham	456.3 ± 21.74	465.4 ± 12.51	505.2 ± 26.41
40/60-S	511.4 ± 22.76	467.2 ± 68.07	526.2 ± 49.55

intermediates or by products.

The use of two or more biopolymers, associated to form interpenetrating networks, complexes, multilayers or fibers is a promising alternative as it does not imply the use of potentially toxic chemicals (Luan et al., 2017; Rahmani Del Bakhshayesh et al., 2018; Li et al., 2018; Bombaldi de Souza et al., 2019). Among these possibilities the formation of polyelectrolyte complexes (PEC), involving a negatively charged polymer and a positively charged polymer is one of the most attractive strategies in terms of gain in mechanical properties without loss of biocompatibility. Chitosan is often used as the positively charged polymer because of its biocompatibility (Periyah et al., 2016) and its easily chemically modifiable structure, mainly to increase its solubility (Tan and Marra, 2010). Concerning the positively charged polymers, the potential choice is greater (Wu et al., 2017). Among possibilities, alginates are frequently used because of their plant origin (unlike collagen) and their widely recognized biocompatibility (Sarker and Boccaccini, 2017; Guarino et al., 2017; Bedian et al., 2017).

Different ways of associating alginate and chitosan have been described in the literature: by mixing at room (Florczyk et al., 2011; Xu et al., 2019; Lv et al., 2019) or higher temperature (Fletcher et al., 2017), bilayer (Banerjee and Ganguly, 2019) or layer by layer (Silva et al., 2017) assemblies, crosslinking (Baysal et al., 2016; Naghizadeha et al., 2018; Zhang et al., 2018), 3D printing (Liu et al., 2018), ... They lead to biocompatible buildings whose mechanical properties can be variable (Francis et al., 2013; Salehi et al., 2019; Lv et al., 2019; Xu et al., 2019), even up to correspond to the mechanical properties of hard tissues (Li et al., 2005; Florczyk et al., 2013). In this context our strategy was to let these biopolymers chemically unmodified, in order to maintain their excellent initial biocompatibility, and to work on the process to obtain a macroporous 3D architecture with improved rheological properties compared with reference polymers. By playing on the mixing conditions and the drying process, we have obtained a family of scaffolds whose mechanical resistance can be adapted to that of soft tissues. Without the use of chemical modifications, porogens or time consuming or expensive processes, we have been able to obtain porous structures that allow deep seeding. After encouraging first results in the cardiac field, we here go further in the characterization of this family of biomaterials and the evaluation their potential as scaffolds aimed to cell

therapy of soft tissues.

In the first part of this study we performed a thorough study of the relationships between chemical structure, 3D morphology and mechanical properties of scaffolds obtained by mixing alginate with chitosan in different proportions. We aimed at clarifying the physico chemical parameters which are likely to affect material cell interactions in 3D. We used micro CT to determine the impact of the preparation method on the morphology of the obtained scaffolds. The micro CT study showed that the PEC, formed as a result of alginate and chitosan interactions, give way after freeze drying to a highly porous material (Fig. 1) with interconnected pores whose diameters were in the range reported to allow cell seeding and vessel ingrowth (Zeltinger et al., 2001; Salem et al., 2002). Comparison of the micro CT slices of the different types of scaffolds suggests that the differences in micro architecture are due to the degree of complexation between the two polymers and 3D distribution of the formed PEC in the bulk material. These differences in chemical composition and in 3D structure impacted the mechanical properties of the scaffolds. Rheological study in dynamic conditions (Fig. 3) highlighted the linear response to cyclic and progressive stimuli. PEC scaffolds presented a visco elastic behavior with predominant elastic properties over a large frequency range (0.01 to 5 Hz) which demonstrates the efficacy of the preparation process to form highly structured polymeric network. The storage modulus increased with chitosan proportion and for 50/50 S and 40/60 S it achieved values greater than that of semi crystalline chitosan gel. Thus, the dynamic analysis at different frequencies highlighted their resistance to strain and elastic behavior. The mechanical test in tension (Fig. 4) showed their capacity to support high level of deformation (up to 50% for 50/50 S) without breaking and preserving a relatively linear response to stress.

The obtained PEC scaffolds stiffness may vary according to alginate/chitosan ratio. Soft tissues mechanical properties reported in the literature have been determined by means of different mechanical testing methods. Tissues elasticities measured by atomic force microscopy span from 0.5 to 1.5 kPa for nerve and liver tissues (Flanagan et al., 2002; Georges et al., 2007) to 5.9 and 8.17 for smooth and skeletal muscle tissues (Engler et al., 2004; Berry et al., 2006; Collinsworth et al., 2002; Engler et al., 2006). Few studies have used tensile tests to determine the elastic modulus of biological tissues. Silver et al. have found that in a tensile test the tendon's elastic modulus was 2.8 kPa (Silver, 2006); Wagenseil et al. have found that the arterial wall presented an elastic modulus of 0.3 to 1 kPa (Wagenseil and Mecham, 2009). The proposed PEC 3D scaffolds, whose tensile elastic moduli are ranging from 0.5 to 1.5 kPa, present mechanical properties answering those of soft tissues.

Under other experimental conditions the increase in Young's modulus obtained by associating alginate and chitosan reaches values

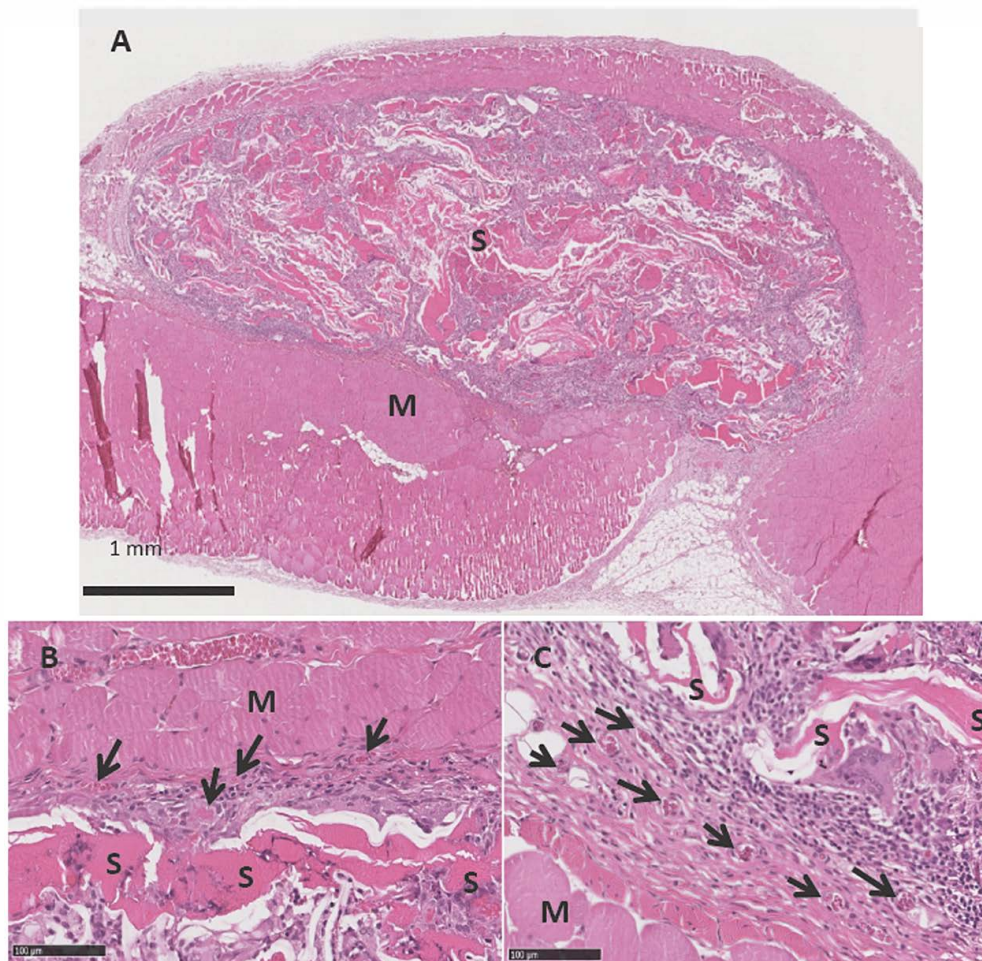


Fig. 9. Implantation of a 40/60 PEC scaffold in a muscle pouch on the pectoral muscle of healthy rats: Host tissue's reaction and graft's fate 28 days after implantation.

Optical micrographs of an implanted 40/60 PEC scaffold harvested 28 days after implantation: A: overview; B and C: zoom to the fibrous capsule formed around the implant. M: muscle; S: scaffold. Black arrows indicate newly-formed blood vessels containing erythrocytes. Scale bars correspond to 1 mm for panel A and to 100 μm for panels B and C.

allowing their use for bone (Park et al., 2013; Florczyk et al., 2013; Li et al., 2005) or cartilage (Qi et al., 2011; Li et al., 2008; Shao and Hunter, 2007; Li and Zhang, 2005) tissue reconstruction. In these studies the Young's modulus is of the order of several MPa, which is about 100 times higher than Young's modulus measured for our scaffolds described here. These notable differences can be explained by the polymer choice (molecular weight, chitosan's degree of acetylation, and alginate's M/G ratio), their respective concentrations in the mix, the final polymer concentration, the type and concentration of the gelling ions and the freezing regime during freeze drying. The variety of properties which can be obtained underlines the importance of polymers and technological process choice.

In view of matrix assisted cell therapy, key parameters to analyze are cell viability, retention and proliferation. These parameters, resulting from the cell material interactions, condition the numbers of functional cells present in the scaffold and determine the long term success of the therapy. We observed that upon rehydration, all scaffolds swelled quickly enough to allow efficient cell seeding thanks to their porosity and hydrophilic character (Fig. 2). Using confocal microscopy examination of double stained cells with calcein and ethidium homo dimer (Fig. 5), a strong prevalence of live cells on dead cells was observed. Moreover, cells were distributed in depth as soon as one day after seeding. Overall, these results confirm that the scaffolds' porous structure, together with the used seeding method, allowed an efficient cell penetration through the thickness of the scaffold. All scaffolds were

biocompatible and favored long term cell culture.

Cell retention capacity was evaluated within 16 h of seeding and then cell number within scaffolds was followed during 14 days. All scaffolds presented an excellent seeding efficiency ($\sim 90\%$) in the first hours after seeding (Fig. 6A). Such a high level of cell retention is understandable because the cells entrapped in the pores of the scaffold had little chance to escape. However, 24 h after seeding, MSC were efficiently retained only within 40/60 S. This sharp drop in cell numbers for 100/0 S and 0/100 S within the first day after seeding could be due to the fact that alginate and chitosan gels are rather fragile physical gels and may be damaged during centrifugation (used for seeding), which entails cell release out of scaffolds.

Over the following days of *in vitro* culture (Fig. 6B), cell number remained close to the number of seeded cells within 40/60 S not only thanks to efficient cell retention but also to cell proliferation, particularly noticeable between day 7 and day 14. In contrast, in the reference scaffolds 100/0 S and 0/100 S, cell number globally decreased.

MSC interactions with 3D PEC scaffolds were examined in this study using SEM microscopy (Fig. 7). Our results revealed that MSC seeded within the 40/60 PEC scaffold established anchoring areas with the substrate through cytoplasmic extensions. Moreover, in a previous publication of our team we have shown by mean of actin vinculin staining and confocal microscopy that the alginate/chitosan ratio 40/60 fostered cell adhesion, contrary to reference alginate (Ceccaldi et al., 2014). Taken together, these observations demonstrate that the studied

scaffold has the potential to provide an appropriate microenvironment for 3D MSC culture and further ensures its biocompatibility.

In addition, we observed in confocal fluorescence microscopy that within PEC scaffolds MSC formed clusters. This cell distribution could be the consequence of the PEC scaffolds' inhomogeneous porosity, observed in micro CT, in terms of pore size and wall thickness, compared to reference scaffolds. It could also be related to the 3D distribution of the opposite charge PECs generated by mixing alginate and chitosan which create zones favoring cell attachment. Although chitosan is known for its good cell adhesion properties (Ceccaldi et al., 2014), the lack of cell proliferation within 0/100 S could be due to its small pore diameter evidenced in microtomography. Another factor contributing to cell loss could be the progressive degradation of the alginate and chitosan hydrogels over the two week culture period.

Our in vitro experiments demonstrated the drastic beneficial effect of PEC formation on MSC ingrowth: the 40/60 S scaffold provided better MSC retention and favored their proliferation during a 2 week culture. FGF2 quantification in the medium of cell seeded scaffolds showed that this factor is efficiently secreted without major interaction with the biopolymers constituting the scaffold. Moreover, 40/60 PEC scaffolds have a tendency to promote FGF2 MSC secretion ability.

In the second part of this study, we assessed the biocompatibility of the PEC scaffold by intramuscular implantation on healthy rats. Biocompatibility of engineered scaffolds is a critical issue for the long term efficacy of this therapeutic approach. Although a consistent body of literature exists on alginate's and chitosan's biocompatibility upon implantation (Guarino et al., 2015), it was necessary to assess the biocompatibility of the scaffolds prepared in this study. Quantification of plasmatic CRP and hematology analyses demonstrated the lack of chronic inflammation secondary to implantation. During the one month follow up (Fig. 9), the scaffold degraded progressively without immune exacerbation. Neovascularization is another critical point which determines the success of tissue engineering on the long term. As a consequence, the numerous newly formed blood vessels we observed 1 month after implantation is one more element demonstrating the beneficial interest of the scaffolds we developed for soft tissues cell therapy.

The selected approach allows taking advantage of MSC paracrine secretions (rather than their ability to migrate and integrate the tissue), and concentrating the cells close to the therapeutic target via a 3D scaffold.

The selected biopolymers, alginate and chitosan, can be provided in clinical grade and their well known biomimicry and biocompatibility, unmodified after engineering, ensures the possibility of a rapid transfer of the scaffolds to a clinical evaluation (Dornish et al., 2001). The described scaffolds are easy to produce, with good reproducibility, at relatively low cost and using commercially available technologies. In their dry form they have a long conservation time life and convenient for off the shelf use.

The biomaterial fabrication makes use of smooth engineering procedures, and the scaffold physical characteristics can be designed to improve cell retention, survival, and interactions with the surrounding tissue as well as to facilitate handle during surgical implantation.

Our team has already shown the potential therapeutic properties of biomaterial assisted MSC implantation in kidney and heart (Trouche et al., 2010; Ceccaldi et al., 2014). The scaffolds described here could suit a variety of soft tissues such as skeletal muscle, lung, liver, and kidney thanks to the possibility to play with chemical composition to obtain scaffolds with tailorable stiffness/elasticity and porosity.

5. Conclusion

In this study we showed that alginate chitosan scaffolds are valuable candidates permitting to promote MSC viability and ease of implantation for soft tissue cell treatment. We developed a 3D porous scaffold with suitable porous architecture and mechanical properties using

naturally derived biomaterials which, combined with MSC, could be used for cell therapy of ischemic disorders. Our strategy is an attractive way to take advantage of the MSC's paracrine effects and is original for the soft tissue engineering field.

Declaration of Competing Interest

The authors declare that they have no known competing financial interests or personal relationships that could have appeared to influence the work reported in this paper.

Acknowledgments

This work was supported by INSERM and Région Midi Pyrénées grants. We wish to thank the Cellular Imaging Facility (T.R.I. Genotoul Plateform, Toulouse, France) and the FERMAT federation for X ray tomography facilities.

References

- Ahmed, T.A., Hincke, M.T., 2014 Jun. Mesenchymal stem cell-based tissue engineering strategies for repair of articular cartilage. *Histol. Histopathol.* 29 (6), 669–689.
- Amsalem, Y., Mardor, Y., Feinberg, M.S., et al., 2007 Sep 11. Iron-oxide labeling and outcome of transplanted mesenchymal stem cells in the infarcted myocardium. *Circulation* 116 (11 Suppl), I38–I45.
- Asgharia, F., Samieia, M., Adibkia, K., et al., 2017. Biodegradable and biocompatible polymers for tissue engineering application: a review. *Artif. Cells Nanomed. Biotechnol.* 45 (2), 185–192.
- Azad, A.K., Sermsintham, N., Chandkrachang, et al., 2004. Chitosan membrane as a wound-healing dressing: characterization and clinical application. *J. Biomed. Mater. Res. B Appl. Biomater.* 69 (2), 216–222 (May 15).
- Banerjee, A., Ganguly, S., 2019. Alginate–chitosan composite hydrogel film with macrovoids in the inner layer for biomedical applications. *J. Appl. Polym. Sci.* 47599.
- Bartunek, J., Behfar, A., Dolatabadi, D., et al., 2013. Cardiopoietic stem cell therapy in heart failure: the C-CURE (Cardiopoietic stem Cell therapy in heart failure) multicenter randomized trial with lineage-specified biologics. *J. Am. Coll. Cardiol.* 61 (23), 2329–2338.
- Baysal, K., Aroguz, A.Z., Adiguzel, Z., Baysal, B.M., 2016. Chitosan/alginate crosslinked hydrogels: preparation, characterization and application for cell growth purposes. *Int. J. Biol. Macromol.* 59, 342–348.
- Bedian, L., Villalba-Rodríguez, A.M., Hernández-Vargas, G., et al., 2017. Bio-based materials with novel characteristics for tissue engineering applications – a review. *Int. J. Biol. Macromol.* 98, 837–846.
- Berry, M.F., Engler, A.J., Woo, Y.J., et al., 2006. Mesenchymal stem cell injection after myocardial infarction improves myocardial compliance. *Am. J. Physiol. Heart Circ. Physiol.* 290, H2196–H2203.
- Bombaldi de Souza, R.F., Bombaldi de Souza, F.C., Rodrigues, C., et al., 2019. Mechanically-enhanced polysaccharide-based scaffolds for tissue engineering of soft tissues. *Mater. Sci. Eng. C* 94, 364–375.
- Ceccaldi, C., Fullana, S.G., Alfarano, C., et al., 2012. Alginate scaffolds for mesenchymal stem cell cardiac therapy: influence of alginate composition. *Cell Transplant.* 21 (9), 1969–1984.
- Ceccaldi, C., Bushkalova, R., et al., 2014. Evaluation of polyelectrolyte complex-based scaffolds for mesenchymal stem cell therapy in cardiac ischemia treatment. *Acta Biomater.* 10 (2), 901–911.
- Ceccaldi, C., Bushkalova, R., Cussac, D., et al., 2017. Elaboration and evaluation of alginate foam scaffolds for soft tissue engineering. *Int. J. Pharm.* 524 (1–2), 433–442.
- Chen, X.W., Zhu, D.J., Ju, Y.L., et al., 2012 Oct. Therapeutic effect of transplanting magnetically labeled bone marrow stromal stem cells in a liver injury rat model with 70%-hepatectomy. *Med. Sci. Monit.* 18 (10), BR375–82.
- Cheng, K., Rai, P., Plagov, A., Lan, X., et al., 2013 Jun. Transplantation of bone marrow-derived MSCs improves cisplatin-induced renal injury through paracrine mechanisms. *Exp. Mol. Pathol.* 94 (3), 466–473.
- Chopp, M., Li, Y., Zhang, Z.G., 2009. Mechanisms underlying improved recovery of neurological function after stroke in the rodent after treatment with neurorestorative cell-based therapies. *Stroke* 40 (3 Suppl), S143–S145 (Mar).
- Collinsworth, A.M., Zhang, S., Kraus, W.E., Truskey, G.A., 2002. Apparent elastic modulus and hysteresis of skeletal muscle cells throughout differentiation. *Am. J. Phys. Cell Physiol.* 283, C1219–C1227.
- Dornish, M., Kaplan, D., Skaugrud, O., 2001. Standards and guidelines for biopolymers in tissue-engineered medical products: ASTM alginate and chitosan standard guides. *Ann. N. Y. Acad. Sci.* 944, 388–397.
- Dvir, T., Kedem, A., Ruvinov, E., et al., 2009. Prevascularization of cardiac patch on the omentum improves its therapeutic outcome. *Proc. Natl. Acad. Sci. U. S. A.* 106 (35), 14990–14995.
- Dvir-Ginzberg, M., Elkayam, T., Cohen, S., 2008 May. Induced differentiation and maturation of newborn liver cells into functional hepatic tissue in macroporous alginate scaffolds. *FASEB J.* 22 (5), 1440–1449.
- Engler, A.J., Richert, L., Wong, J.Y., et al., 2004. Surface probe measurements of the elasticity of sectioned tissue, thin gel sand polyelectrolyte multilayer films:

- correlations between substrate stiffness and cell adhesion. *Surf. Sci.* 570, 142–154.
- Engler, A.J., Sen, S., Sweeney, H.L., et al., 2006. Matrix elasticity directs stem cell lineage specification. *Cell* 126 (4), 677–689.
- Feygin, J., Mansoor, A., Eckman, P., et al., 2007 Sep. Functional and bioenergetic modulations in the infarct border zone following autologous mesenchymal stem cell transplantation. *Am. J. Physiol. Heart Circ. Physiol.* 293 (3), H1772–H1780.
- Flanagan, L.A., Ju, Y.E., Marg, B., Osterfield, M., Janney, P.A., 2002. Neurite branching on deformable substrates. *Neuroreport* 13, 2411–2415.
- Fletcher, N.A., Von Nieda, E.L., Krebs, M.D., 2017. Cell-interactive alginate-chitosan biopolymer systems with tunable mechanics and antibody release rates. *Carbohydr. Polym.* 175, 765–772.
- Florczyk, S.J., Kim, D.J., Wood, D.L., et al., 2011. Influence of processing parameters on pore structure of 3D porous chitosan-alginate polyelectrolyte complex scaffolds. *J. Biomed. Mater. Res. Part A* 98A, 614–620.
- Florczyk, S.J., Leung, M., Li, Z., et al., 2013. Evaluation of three-dimensional porous chitosan-alginate scaffolds in rat calvarial defects for bone regeneration applications. *J. Biomed. Mater. Res. A* 101 (10), 2974–2983.
- Francis, N.L., Hunger, P.M., Donius, A.E., et al., 2013. An ice-templated, linearly aligned chitosan-alginate scaffold for neural tissue engineering. *J. Biomed. Mater. Res. A* 101 (12), 3493–3503.
- Gao, J., Liu, R., Wu, J., et al., 2012 May. The use of chitosan based hydrogel for enhancing the therapeutic benefits of adipose-derived MSCs for acute kidney injury. *Biomaterials* 33 (14), 3673–3681.
- Georges, P.C., Hui, J.J., Gombos, Z., McCormick, M.E., Wang, A.Y., Uemura, M., Mick, R., Janney, P.A., Furth, E.E., Wells, R.G., 2007. Increased stiffness of the rat liver precedes matrix deposition: implications for fibrosis. *Am. J. Physiol. Gastro-intest. Liver Physiol.* 293, G1147–G1154.
- Gnavi, S., Barwig, C., Freier, T., et al., 2013. The use of chitosan-based scaffolds to enhance regeneration in the nervous system. *Int. Rev. Neurobiol.* 109, 1–62.
- Gnecchi, M., He, H., Noiseux, N., et al., 2006. Evidence supporting paracrine hypothesis for Akt-modified mesenchymal stem cell-mediated cardiac protection and functional improvement. *FASEB J.* 20 (6), 661–669.
- Guarino, V., Caputo, T., Altobelli, R., Ambrosio, L., 2015. Degradation properties and metabolic activity of alginate and chitosan polyelectrolytes for drug delivery and tissue engineering applications. *AIMS Mater. Sci.* 2 (4), 497–502.
- Guarino, V., Altobelli, R., Sala, F., et al., 2017. Alginate processing routes to fabricate bioinspired platforms for tissue engineering and drug delivery. *Algin. Biomed. Appl.* 9 (4), 101–120.
- Hare, J.M., Traverse, J.H., Henry, T.D., et al., 2009. A randomized, double-blind, placebo-controlled, dose-escalation study of intravenous adult human mesenchymal stem cells (prochymal) after acute myocardial infarction. *J. Am. Coll. Cardiol.* 54 (24), 2277–2286.
- Hussain, A., Collins, G., Yip, D., Cho, C.H., 2013 Feb. Functional 3-D cardiac co-culture model using bioactive chitosan nanofiber scaffolds. *Biotechnol. Bioeng.* 110 (2), 637–647.
- Kaiser, N.J., Coulombe, K.L.K., 2015. Physiologically inspired cardiac scaffolds for tailored in vivo function and heart regeneration. *Biomed. Mater.* 10, 034003.
- Karantalis, V., DiFede, D.L., Gerstenblith, G., et al., 2014. Autologous mesenchymal stem cells produce concordant improvements in regional function, tissue perfusion, and fibrotic burden when administered to patients undergoing coronary artery bypass grafting: the prospective randomized study of mesenchymal stem cell therapy in patients undergoing cardiac surgery (PROMETHEUS) trial. *Circ. Res.* 114 (8), 1302–1310.
- Kim, S.S., Park, H.J., Han, J., et al., 2003 Sep. Renal tissue reconstitution by the implantation of renal segments on biodegradable polymer scaffolds. *Biotechnol. Lett.* 25 (18), 1505–1508.
- Leor, J., Abouafia-Etzion, S., Dar, A., et al., 2000. Bioengineered cardiac grafts: a new approach to repair the infarcted myocardium? *Circulation* 102 (19 Suppl 3), III56–61.
- Lev, R., Seliktar, D., 2018. Hydrogel biomaterials and their therapeutic potential for muscle injuries and muscular dystrophies. *J. R. Soc. Interface* 15, 20170380.
- Li, Z., Zhang, M., 2005. Chitosan-alginate as scaffolding material for cartilage tissue engineering. *J. Biomed. Mater. Res. A* 75 (2), 485–493.
- Li, Z., Ramay, H.R., Hauch, K.D., et al., 2005. Chitosan-alginate hybrid scaffolds for bone tissue engineering. *Biomaterials* 26 (18), 3919–3928.
- Li, Z., Gunn, J., Chen, M.H., et al., 2008. On-site alginate gelation for enhanced cell proliferation and uniform distribution in porous scaffolds. *J. Biomed. Mater. Res. A* 86 (2), 552–559.
- Li, D., Zhang, M., Zhang, Q., et al., 2015 May. Functional recovery after acute intravenous administration of human umbilical cord mesenchymal stem cells in rats with cerebral ischemia-reperfusion injury. *Intractable Rare Dis. Res.* 4 (2), 98–104.
- Li, H., Hu, C., Yu, H., et al., 2018. Chitosan composite scaffolds for articular cartilage defect repair: a review. *RSC Adv.* 8, 3736.
- Li, L., Yu, F., Zheng, L., et al., 2019. Natural hydrogels for cartilage regeneration: modification, preparation and application. *J. Orthopaedic. Transl.* 17, 26–41.
- Liu, Q., Li, Q., Xu, S., et al., 2018. Preparation and properties of 3d printed alginate-chitosan polyion complex hydrogels for tissue engineering. *Polymers* 10, 664.
- Liu, S., Xie, Y.Y., Wang, B., 2019. Role and prospects of regenerative biomaterials in the repair of spinal cord injury. *Neural Regen. Res.* 14 (8), 1352–1363.
- Luan, C., Liu, P., Chen, R., Chen, B., 2017. Hydrogel based 3D carriers in the application of stem cell therapy by direct injection. *Nanotechnol. Rev.* 6 (5), 435–448.
- Lv, X., Liu, Y., Song, S., 2019. Influence of chitosan oligosaccharide on the gelling and wound healing properties of injectable hydrogels based on carboxymethyl chitosan/alginate polyelectrolyte complexes. *Carbohydr. Polym.* 205, 312–321.
- Mäkelä, T., Takalo, R., Arvola, O., et al., 2015. Safety and biodistribution study of bone marrow-derived mesenchymal stromal cells and mononuclear cells and the impact of the administration route in an intact porcine model. *Cytherapy* 0, 1e11.
- Malafaya, P.B., Reis, R.L., 2009 Feb. Bilayered chitosan-based scaffolds for osteochondral tissue engineering: influence of hydroxyapatite on in vitro cytotoxicity and dynamic bioactivity studies in a specific double-chamber bioreactor. *Acta Biomater.* 5 (2), 644–660.
- Malliaras, K., Marbán, E., 2011. Cardiac cell therapy: where we've been, where we are, and where we should be headed. *Br. Med. Bull.* 98 (1), 161–185.
- Mias, C., Trouche, E., Seguelas, M.H., et al., 2008. Ex vivo pretreatment with melatonin improves survival, proangiogenic/mitogenic activity, and efficiency of mesenchymal stem cells injected into ischemic kidney. *Stem Cells* 26 (7), 1749–1757.
- Mias, C., Lairez, O., Trouche, E., et al., 2009. Mesenchymal stem cells promote matrix metalloproteinase secretion by cardiac fibroblasts and reduce cardiac ventricular fibrosis after myocardial infarction. *Stem Cells* 27 (11), 2734–2743.
- Morigi, M., Introna, M., Imberti, B., et al., 2008. Human bone marrow mesenchymal stem cells accelerate recovery of acute renal injury and prolong survival in mice. *Stem Cells* 26 (8), 2075–2082.
- Naghizadeha, Z., Karkhaneha, A., Khojastehb, A., 2018. Self-crosslinking effect of chitosan and gelatin on alginate based hydrogels: injectable in situ forming scaffolds. *Mater. Sci. Eng. C* 175, 256–264.
- Newsom, J.P., Payne, K.A., Krebs, M.D., 2019. Microgels: modular, tunable constructs for tissue regeneration. *Acta Biomater.* 88, 32–41.
- Noronha, N.C., Amanda Mizukami, A., Carolina Caláiri-Oliveira, C., et al., 2019. Priming approaches to improve the efficacy of mesenchymal stromal cell-based therapies. *Stem Cell Res. Ther.* 10, 131.
- Oryana, A., Kamalia, A., Moshiric, A., et al., 2018. Chemical crosslinking of biopolymeric scaffolds: current knowledge and future directions of crosslinked engineered bone scaffolds. *Int. J. Biol. Macromol.* 107, 678–688.
- Pan, G.Z., Yang, Y., Zhang, J., et al., 2012 Dec. Bone marrow mesenchymal stem cells ameliorate hepatic ischemia/reperfusion injuries via inactivation of the MEK/ERK signaling pathway in rats. *J. Surg. Res.* 178 (2), 935–948.
- Park, H., Choi, B., Nguyen, J., Fan, et al., 2013. Anionic carbohydrate-containing chitosan scaffolds for bone regeneration. *Carbohydr. Polym.* 97 (2), 587–596.
- Perez, R.A., Jung, C.R., Kim, H.W., 2017. Biomaterials and culture technologies for regenerative therapy of liver. *Tissue. Adv. Healthcare Mater.* 6, 1600791.
- Perez-Estena, I., Prosper, F., Pelacho, B., 2018. Allogeneic mesenchymal stem cells and biomaterials: the perfect match for cardiac repair? *Int. J. Mol. Sci.* 19, 3236.
- Periyah, M.H., Halim, A.S., Saad, A.Z.M., 2016. Chitosan: a promising marine polysaccharide for biomedical research. *Pharmacogn. Rev.* 10 (19), 39–42.
- Perin, E.C., Silva, G.V., Assad, J.A., et al., 2008. Comparison of intracoronary and transcatheter delivery of allogeneic mesenchymal cells in a canine model of acute myocardial infarction. *J. Mol. Cell. Cardiol.* 44 (3), 486–495.
- Poitevin, S., Cussac, D., Leroyer, A.S., et al., 2014. Sphingosine kinase 1 expressed by endothelial colony-forming cells has a critical role in their revascularization activity. *Cardiovasc. Res.* 103 (1), 121–130.
- Qi, S., Wu, D., 2013 Dec. Bone marrow-derived mesenchymal stem cells protect against cisplatin-induced acute kidney injury in rats by inhibiting cell apoptosis. *Int. J. Mol. Med.* 32 (6), 1262–1272. <https://doi.org/10.3892/ijmm.2013.1517>.
- Qi, J., Chen, A., You, H., et al., 2011. Proliferation and chondrogenic differentiation of CD105-positive enriched rat synovium-derived mesenchymal stem cells in three-dimensional porous scaffolds. *Biomed. Mater.* 6 (1), 015006.
- Rahmani Del Bakhshayesh, A., Annabi, N., Khalilov, R., et al., 2018. Recent advances on biomedical applications of scaffolds in wound healing and dermal tissue engineering. *Artif. Cells Nanomed. Biotechnol.* 46 (4), 691–705.
- Rane, A.A., Christman, K.L., 2011. Biomaterials for the treatment of myocardial infarction. A 5-year update. *J. Am. Coll. Cardiol.* 58 (25), 2615–2629.
- Reis, L.A., Borges, F.T., Simões, M.J., et al., 2012. Bone marrow-derived mesenchymal stem cells repaired but did not prevent gentamicin-induced acute kidney injury through paracrine effects in rats. *PLoS One* 7 (9), e44092.
- Saberianpour, S., Heidarzadeh, M., Geranmayeh, M.H., et al., 2018. Tissue engineering strategies for the induction of angiogenesis using biomaterials. *J. Biol. Eng.* 12, 36.
- Salehi, M., Bagher, Z., Kamrava, S.K., 2019. Alginate/chitosan hydrogel containing olfactory ectomesenchymal stem cells for sciatic nerve tissue engineering. *J. Cell. Physiol.* 234, 15357–15368.
- Salem, A.K., Stevens, R., Pearson, R.G., et al., 2002. Interactions of 3T3 fibroblasts and endothelial cells with defined pore features. *J. Biomed. Mater. Res.* 61 (2), 212–217.
- Sarker, B., Boccacini, A.R., 2017. Alginate utilization in tissue engineering and cell therapy. *Algin. Biomed. Appl.* 9 (5), 121–155.
- Shachar, M., Tsur-Gang, O., Dvir, T., et al., 2011. The effect of immobilized RGD peptide in alginate scaffolds on cardiac tissue engineering. *Acta Biomater.* 7 (1), 152–162.
- Shao, X., Hunter, C.J., 2007. Developing an alginate/chitosan hybrid fiber scaffold for annulus fibrosus cells. *J. Biomed. Mater. Res. A* 82 (3), 701–710.
- Sholugu, N., Scully, M., Laffey, J.G., et al., 2018. Human mesenchymal stem cell secretome from bone marrow or adipose-derived tissue sources for treatment of hypoxia-induced pulmonary epithelial injury. *Int. J. Mol. Sci.* 19 (10), 2996.
- Silva, J.M., Garcia, J.R., Reis, R.L., et al., 2017. Tuning cell adhesive properties via layer-by-layer assembly of chitosan and alginate. *Acta Biomater.* 51, 279–293.
- Silver, F.H., 2006. Mechanosensing and Mechanochemical Transduction in Extracellular Matrix: Biological, Chemical, Engineering, and Physiological Aspects. Springer Science.
- Souidi, N., Stolk, M., Seifert, M., 2013. Ischemia-reperfusion injury: beneficial effects of mesenchymal stromal cells. *Curr. Opin. Organ Transplant.* 18, 34–43.
- Tan, H., Marra, K.G., 2010. Injectable, biodegradable hydrogels for tissue engineering applications. *Materials* 3 (3), 1746–1767.
- Tiwari, S., Patil, R., Bahadur, P., 2019. Polysaccharide based scaffolds for soft tissue engineering applications. *Polymers* 11, 1.
- Tögel, F.E., Westenfelder, C., 2012. Kidney protection and regeneration following acute injury: progress through stem cell therapy. *Am. J. Kidney Dis.* 60 (6), 1012–1022

- (Dec).
- Toma, C., Pittenger, M.F., Cahill, K.S., et al., 2002. Human mesenchymal stem cells differentiate to a cardiomyocyte phenotype in the adult murine heart. *Circulation* 105 (1), 93–98.
- Trouche, E., Girod Fullana, S., Mias, C., et al., 2010. Evaluation of alginate microspheres for mesenchymal stem cell engraftment on solid organ. *Cell Transplant.* 19, 1623–1633.
- Wagenseil, J.E., Mecham, R.P., 2009. Vascular extracellular matrix and arterial mechanics. *Physiol. Rev.* 89 (3), 957–989.
- Wang, H., Zhang, X., Li, Y., et al., 2010. Improved myocardial performance in infarcted rat heart by co-injection of basic fibroblast growth factor with temperature-responsive chitosan hydrogel. *J. Heart Lung Transplant.* 29 (8), 881–887.
- Wang, W., Du, Z., Yan, J., et al., 2014. Mesenchymal stem cells promote liver regeneration and prolong survival in small-for-size liver grafts: involvement of C-Jun N-terminal kinase, cyclin D1, and NF- κ B. *PLoS One* 9 (12), e112532 (Dec 5).
- Williams, A.R., Hare, J.M., 2011. Mesenchymal stem cells: biology, pathophysiology, translational findings, and therapeutic implications for cardiac disease. *Circ. Res.* 109 (8), 923–940.
- Wu, T., Li, Y., Lee, D.S., 2017. Chitosan-based composite hydrogels for biomedical applications. *Macromol. Res.* 25 (6), 480–488.
- Xu, K., Ganapathy, K., Andl, T., et al., 2019. 3D porous chitosan-alginate scaffold stiffness promotes differential responses in prostate cancer cell lines. *Biomaterials* 217, 119311.
- Zahir, T., Nomura, H., Guo, X.D., et al., 2008. Bioengineering neural stem/progenitor cell-coated tubes for spinal cord injury repair. *Cell Transplant.* 17 (3), 245–254.
- Zeltinger, J., Sherwood, J.K., Graham, D.A., et al., 2001. Effect of pore size and void fraction on cellular adhesion, proliferation, and matrix deposition. *Tissue Eng.* 7 (5), 557–572.
- Zhang, L., Fang, H., Zhang, K., Yin, J., 2018. Homologous sodium alginate/chitosan-based scaffolds, but contrasting effect on stem cell shape and osteogenesis. *ACS Appl. Mater. Interfaces* 10, 6930–6941.
- Zieber, L., Or, S., Ruvinov, E., et al., 2014. Microfabrication of channel arrays promotes vessel-like network formation in cardiac cell construct and vascularization in vivo. *Biofabrication* 6 (2), 024102.
- Zmora, S., Glicklis, R., Cohen, S., 2002. Tailoring the pore architecture in 3-D alginate scaffolds by controlling the freezing regime during fabrication. *Biomaterials* 23 (20), 4087–4094.